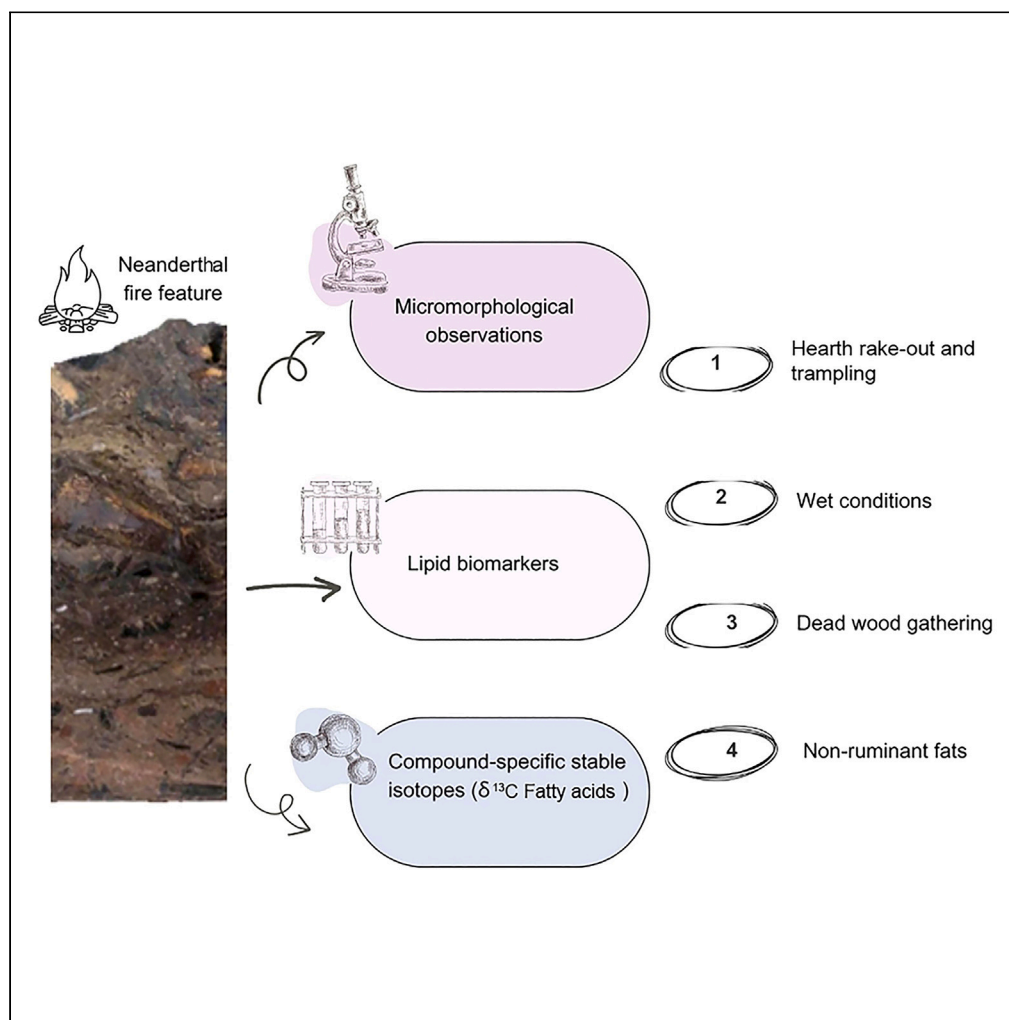# iScience

Article

Microstratigraphic, lipid biomarker and stable isotope study of a middle Palaeolithic combustion feature from Axlor, Spain

Margarita Jambrina-Enríquez, Carolina Mallol, Antonio V. Herrera Herrera, Jesús Gonzalez-Urquijo, Talía Lazuen

mjambrin@ull.edu.es

Highlights

Microcontextual study was performed on a Middle Paleolithic combustion feature

Micromorpology and lipid biomarkers studies inform about Neanderthal pyroarchaeology

Micromorphological features reveal human activities such as hearth rake-out and trampling

Lipid biomarkers unveil non-ruminant fats and dead-wood components in combustion residues

Article

Microstratigraphic, lipid biomarker and stable isotope study of a middle Palaeolithic combustion feature from Axlor, Spain

Margarita Jambrina-Enríquez,[1,2,8,9,*] Carolina Mallol,[2,3,4,8] Antonio V. Herrera Herrera,[2,5] Jesús Gonzalez-Urquijo,[6] and Talía Lazuen[6,7]

SUMMARY

Archaeological research has increasingly focused on studying combustion features as valuable sources of information regarding past technological and cultural aspects. The use of microstratigraphic and biomolecular techniques enables the identification of combustion residues and substrate components, and infer about past fire-related activities and the environments. Our study conducted on a combustion feature (Level N, ∼100 Ka) at the Axlor cave, a Middle Paleolithic site in northern Iberia, exemplifies the interdisciplinary approach to combustion features. Micromorphological features revealed depositional activities associated with occupations such as hearth rake-out and trampling. Through molecular (*n*-alkanes, *n*-alcohols, and *n*-fatty acids) and isotopic analysis ($\delta^{13}C_{16:0}$ and $\delta^{13}C_{18:0}$), we infer the good preservation of organic matter, the contributions of non-ruminant fats, and the dead-wood gathering strategies by Neanderthal groups. By combining microstratigraphic and biomolecular approaches, our study significantly contributes to the advancement of our current understanding of Neanderthal pyrotechnology.

INTRODUCTION

Combustion features are key archaeological sedimentary deposits comprising combustion residues (charcoal, phytoliths, and heated bone, stone or pottery) and thermally altered sediments.[1,2] In Middle Paleolithic research, they are especially relevant given their prominence in the archaeological record and provide us with information on the technological, economic and cultural aspects of some of the activities carried out by different human groups.[3–5] The current data from different sites throughout Iberia indicate that Iberian Neanderthals used different species of wood as fuel depending on the availability of wood in the forests in the immediate vicinity of the sites (pine or thermomediterranean species); in addition to local availability, fuel gathering preferences appear to have involved the state and caliber of the wood.[4] Alternative fuels such as animal fat, bones, resin, leaves, and pinecones were also used as a complement to primary fuels, as well as for ignition and maintenance.[4] Archaeological combustion features can represent intact combustion activity contexts (e.g., combustion residues on a ground surface) or contexts reworked by humans, wind, or water (i.e., redeposited combustion residues).[2] Their identification and characterization in the field is difficult due to the complexity of archaeological site formation processes.[6] Interdisciplinary microcontextual approaches have shown high potential to infer past fire-related activities and contribute to the behavioral information of past human societies as well as to reconstruct past environments.[7] Using soil micromorphology in conjunction with other high-resolution analytical techniques can help identify combustion residues and their microstratigraphic relationships.[8]

Over the last few years, Gas Chromatography-Mass Spectrometry (GC-MS) and Gas Chromatography Combustion Isotope Ratio Mass Spectrometry (GC-C-IRMS) high-resolution analyses have been performed on sedimentary deposits associated to combustion features to address the organic residues sources.[9–16] Particularly, the lipid biomarker study on black layers (the charred ground beneath the fire[11]), both in experimental[17–19] and in archaeological[11–16] samples have shown the high preservation of lipid biomarker fingerprint on charred organic matter. This is related to the shielding of organic matter from oxidation and microbial activity when it is subjected to incomplete

[1]Departamento de Biología Animal, Edafología y Geología, Unidad Departamental de Petrología y Geoquímica, Facultad de Ciencias, Universidad de La Laguna, 38200 San Cristóbal de La Laguna, Tenerife, Spain
[2]Archaeological Micromorphology and Biomarker Research Lab (AMBI Lab), Instituto Universitario de Bio-Orgánica Antonio González, Universidad de La Laguna, 38200 San Cristóbal de La Laguna, Tenerife, Spain
[3]Departamento de Geografía e Historia, Unidad Departamental de Prehistoria, Facultad de Humanidades, Universidad de La Laguna, 38200 San Cristóbal de La Laguna, Tenerife, Spain
[4]ICArEHB - Interdisciplinary Center for Archaeology and the Evolution of Human Behaviour, Universidade do Algarve, 8005-139 Faro, Portugal
[5]Departamento de Química, Unidad Departamental de Química Analítica, Facultad de Ciencias, Universidad de La Laguna, 38200 San Cristóbal de La Laguna, Tenerife, Spain
[6]Instituto Internacional de Investigaciones Prehistóricas de Cantabria-IIIPC (UC, Santander, Gobierno de Cantabria), Universidad de Cantabria, 39005 Santander, Spain
[7]Université de Bordeaux, CNRS, MCC, UMR 5199 - PACEA, Pessac, France
[8]These authors contributed equally
[9]Lead contact
*Correspondence: mjambrin@ull.edu.es
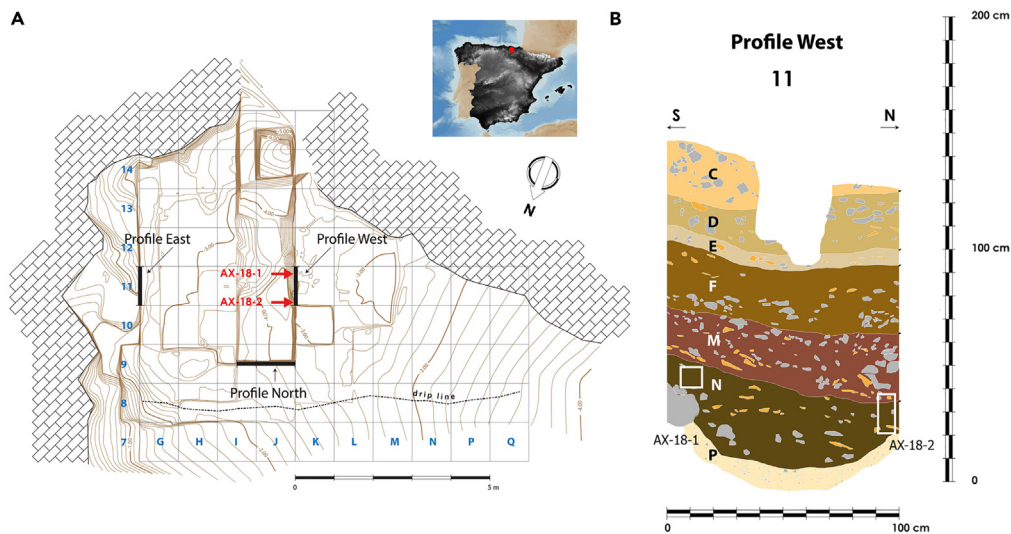https://doi.org/10.1016/j.isci.2023.108755

Figure 1. Study site and profiles location
(A) Map showing the location of Axlor Cave in the northern Iberian Peninsula and plan view of the excavated area showing the location of the West profile.
(B) West profile showing the location of the micromorphological and biomarker samples included in this study (AX-18-1 and AX-18-2).

combustion under limited oxygen conditions and below 400°C.[18–23] The average temperature of $\leq 300°C$ associated with black sedimentary layers (between 2 and 10 cm depth)[11,17,23] preserve the original biomarker fingerprint providing information about the sources of organic material (plant oils vs. animal fats, different plant tissues, degradation state, gymnosperms vs. angiosperms contributions) helping to better understand the combustion structure function and providing palaeoenvironmental information.[10,11,13–16]

Here, we present a geoarchaeological study of Level N from Axlor, a Middle Palaeolithic site in northern Spain. This is a dark brown sedimentary layer rich in combustion residues (burned bone and charcoal). We conducted soil micromorphology coupled with lipid biomarker analyses including short-chain fatty acid compound-specific carbon stable isotopes ($C_{16:0}$ and $C_{18:0}$). The goal was to explore the formation of this level and obtain behavioral and paleoenvironmental information that could advance our current knowledge on Neanderthal pyrotechnology.

The site of Axlor (43° 07.3′ N, 02° 43.7′ W; 315 m about sea level) is located in the narrow coastal corridor that forms the north Atlantic Iberia region (Figure 1A). The site is close to the present-day coastline (approx. 30 km) but in a very rugged mountainous environment. The cave was formed in the small supra-urgonian karst of Indusi (Dima, Bizkaia, Basque Country). It opens on the third floor, about 20 m above the currently active karstic network. The sedimentary fillings almost completely filled the cavity at the end of the Pleistocene. Axlor site preserves one of the most complete Mousterian sequences of north Atlantic Iberia, extended along the MIS 5 to 3 stages. The sequence is well dated by a battery of single-grain OSL dating.[24] The lithic industry and the repertoire of hunted fauna register important changes over time.[25–27] The sequence contains about ten Neanderthal human remains, frequently dental; two of them, a young adult premolar and a decidual canine of a child around 10–12 years old were recovered in Level N, the subject of this study.[28,29]

Level N constitutes the base of the Mousterian sequence and is dated at 99.6 ± 7.6 Ka (a complementary TT-OSL dating provides a statistically indistinguishable date of 95.6 ± 8.7Ka).[30] The overlying level, Level M, which is additionally studied in this work, is dated to 89.0 ± 6.5 ka.[30] Level N reaches more than 40 cm in the outermost zone, although it is gradually wedged until it disappears toward the interior (Figures 1A and 1B). A sedimentological analysis of the level shows the predominance of silts and clays (86%). Coarse sands are particularly scarce (3.7% of the sandy fraction). An important part of the sedimentary fill is of anthropogenic origin. More than 230,000 faunal fragments >4 mm have been recovered, most of which come from Cervus carcasses (∼75% of the identified remains). The lithic industry is very abundant, with a density>20,000 remains per cubic meter. It is composed of flint, quartz and mudstone. In technological terms, Level N is characterized by the use of Levallois and micro Levallois knapping systems, and by the presence of Mousterian points.[31]

At the sampled location on the West excavation profile (Figure 1A), two soil micromorphology samples, AX-18-1 and AX-18-2, were collected approximately 1 m apart (Figure 1B). The AX-18-2, was positioned more toward the cave entrance (outwards) which also included the base of Layer M (Figure 1B). AX-18-1 was positioned closer to the back wall of the cave and contained only Level N, which was also thinner (11 cm compared to 20 cm in AX-18-2). Level N exhibits a 11/20-cm thick sequence of stratified beds of sandy clays with the appearance of a possible combustion feature. This sequence comprises three visible sublayers or facies: at the base a 3-6 cm-thick, light brown sandy clayey facies with bone and charcoal fragments (Facies N3), a 4-8 cm-thick dark brown sandy clayey facies with frequent bone and charcoal fragments (Facies N2), and at the top a 4-8-cm-thick, grayish-brown sandy clayey facies with charcoal and bone fragments (Facies N1). Samples were carved and wrapped in Plaster of Paris to keep them physically intact during transport. Lipid biomarker sediment samples were collected from the same location as the micromorphology samples (Figure 1B). Approximately 3 cm of sediment were scraped from the profile prior to sampling it to avoid possible contamination from microbial biomass. For the identification of organic combustion residues we collected
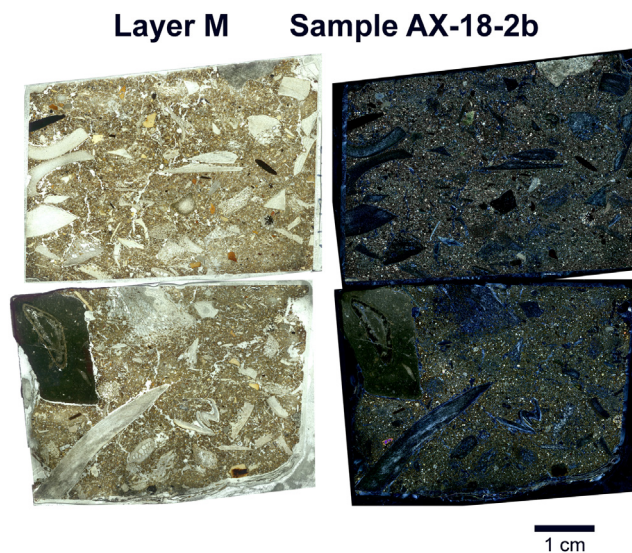
Layer M   Sample AX-18-2b

1 cm

Figure 2. Scans of thin sections from micromorphology sample AX-18-2b (left image in plane polarized light – PPL and right image in crossed polarized light – XPL)

This sample is from the base of Level M. Note the massive, unstratified structure of the deposit and the common presence of unsorted, unburned, cm-sized bone fragments (whitish in PPL and bluish in XPL) and very few sand-sized burned bone fragments (yellow and brown-colored in PPL). The right (XPL) image shows the common presence of quartz sand (small white grains) in this layer.

one sample from each facies of Level N (from bottom to top: N3, N2 and N1) using sterilized tools and wrapped them individually in Al-foil. All the samples were preserved at 4°C prior to laboratory analysis.

RESULTS AND DISCUSSION

Micromorphological observations

The samples show a similar lithological composition of sandy-silty clay with frequent, unsorted quartz silt, very fine sand and medium sand, and minor proportions of quartz coarse sand (Figures 2, 3, and 4). There are also few larger (cm-sized) rounded sandstone fragments. The stratigraphic contacts between Levels M and N and among Facies N1, N2, and N3 are diffuse and each of these is massive, with localized sandy lenses. The matrix in Level N, Facies N2 is rich in amorphous black organic matter, either an isotropic mass or as black stringers within reddish-brown clay (Figures 3, 4, 5A, and 5C). At high magnifications, the N2 black matrix exhibits plant tissue fragments (Figure 5D).

All the samples contain high proportions of poorly sorted bone, with fragments ranging from 0.01 mm to several cm and these are randomly distributed in Level M and arranged in diffuse horizontal beds in Level N (Figures 2, 3, and 4). *In situ*, postdepositional snapping and compression of some of the cm-sized bone fragments are common throughout Level N, particularly at the top of Facies N2 (Figure 3). The bone in basal Level M is not burned except for very few, isolated sand-sized fragments. A relatively high proportion of the bone in all the Level N facies, regardless of size, shows moderate burning, possibly to temperatures in the 200°C–400°C temperature range based on their color[32,33] (Figure 5B). In Facies N3, there are relatively more concentrations of unburned bone fragments than in N2 (Figure 6A). Very few calcined bone fragments were identified throughout Level N (Figure 6B). Anthropogenic cutmarks were observed on a burned bone fragment from Facies N2 (Figures 6C–6E).

Charcoal is present throughout Level N. It is poorly sorted, and angular to subrounded (Figure 6B). A few microscopic vesicular char fragments were identified (Figure 6F), as well as a few charcoal fragments with dense, vesicular portions. A recent microRaman study identified their source as plant.[34] Char fragments are most frequent in Facies N2. Despite of the abundance of fresh burned bone and charcoal, no ash (wood or other) was identified, even in reworked form as microaggregates or microscopic coatings. Some of the bone fragments throughout the samples showed iron staining (Figure 7A).

Microscopic (mm and cm-sized) flint flakes were identified throughout Level N (Figure 7B) but not in Level M. All the Level N facies contain sand-sized fragments of carnivore or omnivore coprolites, some of which are burned (Figures 7C–7F).

Our micromorphological observations allow us to advance some hypotheses about the formation of the Axlor Level N sedimentary beds at the West excavation profile. The lithology of the base of Level M and Level N Facies N1, N2, and N3 point toward low-energy water lain sediment (sandy silty clay) deposited in close temporal association with the human occupation of the site. The macroscopically visible deformation and apparent folding of Level M and N (see Figure 8) suggests that the entire set (Level N) was postdepositionally affected by solifluction or a similar process. The massive structure of the base of Level M suggests that the anthropogenic remains contained in it might be in the secondary position, while the bedding and *in situ* snapping and compression observed throughout the Level N facies indicates the presence of human occupation surfaces at the sampled spots during the formation of each of the Level N facies.
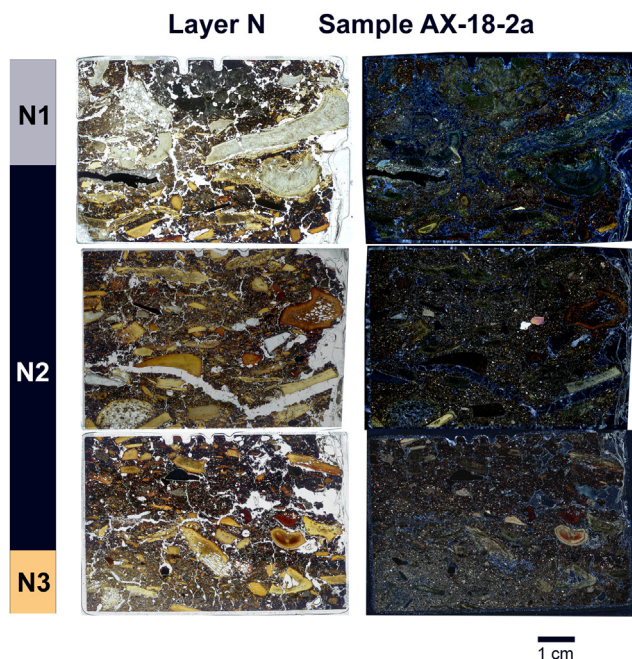
Layer N   Sample AX-18-2a

Figure 3. Scans of thin section from micromorphology sample AX-18-2a (left image in plane polarized light – PPL and right image in crossed polarized light – XPL)

This sample is from Level N, Facies N1, N2 and N3. Note the common presence of diffusely bedded, variably burned, cm-sized bone fragments (yellow and brown/reddish-brown-colored in PPL). Some of these show *in situ* breakage (for instance the two large fragments at the top of N2; center-right of the top thin section). The right (XPL) image shows the common presence of quartz sand (small white grains) in this layer.

Different human activities are represented by the observed microscopic assemblages. The occurrence of cut-marked bone in Level N indicates butchery-related activity, the microscopic flint scatters indicates *in situ* knapping or tool wear, and the co-occurrence of burned bone, charcoal and char indicates combustion activity. However, no microstratigraphic indication of *in situ* combustion (i.e., *in situ* combustion structures) was observed. No ash (from wood or grass) was observed and bone was found in different burning states (unburned, slightly burned, moderately burned, and calcined) at the same stratigraphic positions, suggesting post-combustion reworking. The burned
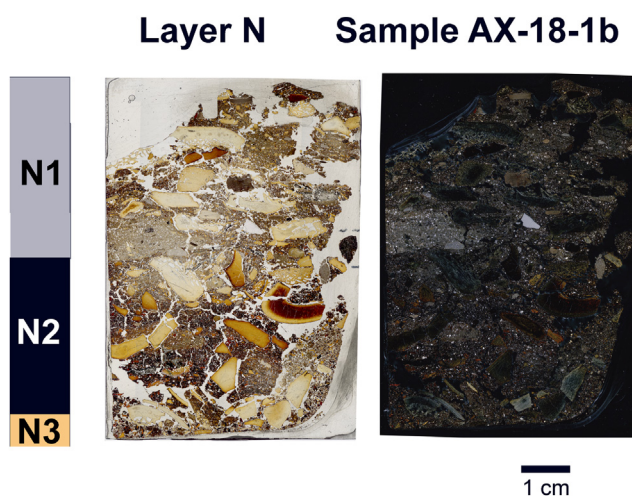
Layer N   Sample AX-18-1b

Figure 4. Scan of thin section AX-18-1b (left image in plane polarized light – PPL and right image in crossed polarized light – XPL)

This sample is from Level N, Facies N1, N2 and N3, which are thinner and more compact than in sample AX-18-2. Note the common presence of diffusely bedded, variably burned, cm-sized bone fragments (yellow and brown/reddish-brown-colored in PPL). Some of these are snapped or compressed *in situ*. The right (XPL) image shows the common presence of quartz sand (small white grains) in this layer and presence of a subangular, cm-sized patch of lighter-colored sandy clay toward the top left.
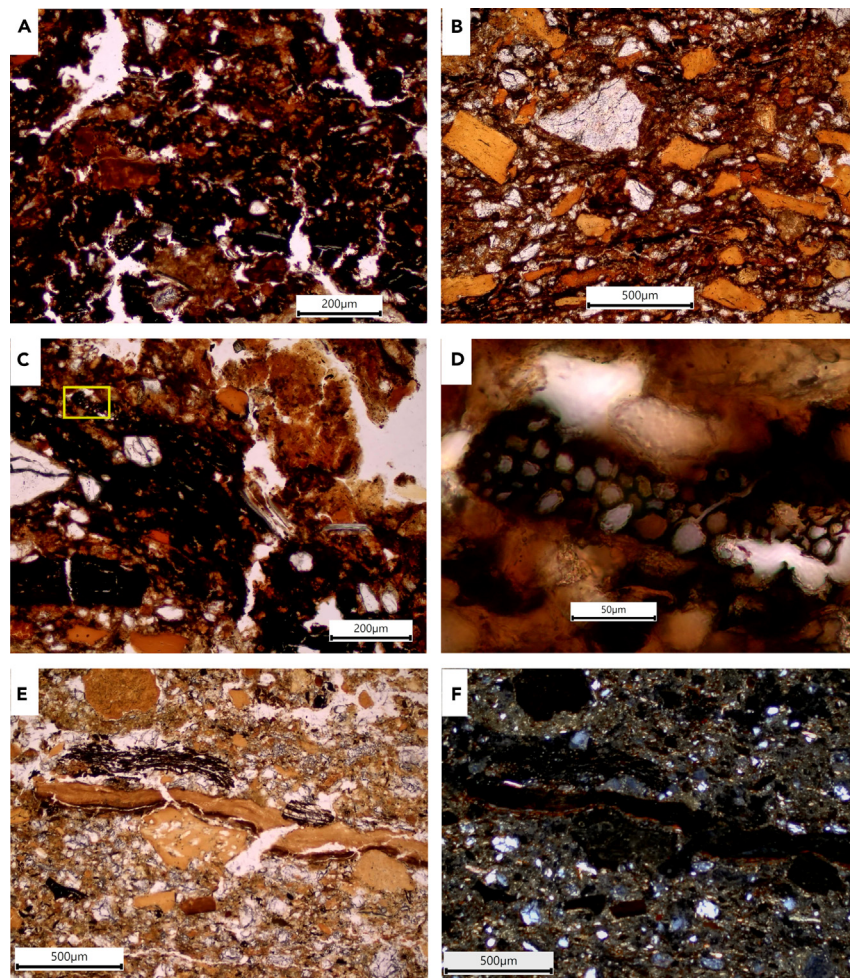
Figure 5. Different microscopic views of the Facies N2 deposit in sample AX-18-1

(A) Black amorphous organic matter intricately mixed into the clayey matrix (PPL).

(B) Common angular-subangular and subrounded sand-sized burned bone fragments (orange colored) and quartz grains in white (PPL).

(C) Black amorphous organic matter with quartz sand (white grains; PPL). The yellow box indicates the position of the image in D.

(D) Detail of plant tissue within the black matrix (yellow box in C) visible at a higher magnification.

(E) Stringer of phosphatic clay (orange colored) observed toward the top of N2 (PPL).

(F) Same as at left but in XPL.

bone-charcoal-char assemblage could be the result of hearth rake out[35] or lateral dispersal through a different process such as animal rummaging, having been subsequently embedded into soft, sandy clayey surfaces through trampling, as evidenced by the occurrence of *in situ* breakage and compression.[35]

Considering the relatively high charcoal content of Facies N2 and the observation of plant tissue at high magnifications, the source of the submillimetric black organic matter in the N2 matrix could be charcoal embedded within wet sedimentary surfaces through trampling during the same human occupations associated with the burned bone assemblages, and possibly derived from the same burning activities. In that case, the lack of blackening above and below Facies N2 could be an indicator of a lower intensity of human occupation or burning activity (less trampling of combustion residues) during the formation of N1 and N3. The presence of coprolites in association with the Level N bone assemblages suggest periods of human abandonment of the site prior to the burial of the bone assemblages, which would also indicate that these are time-averaged palimpsest deposits.

Organic matter sources in the Layer N combustion feature: Lipid biomarker composition and compound-specific stable isotope analysis ($\delta^{13}C_{Faty\ acids}$)

Low-polar compounds including *n*-alkanes, polycyclic aromatic hydrocarbons (PAHs), *n*-ketones, *n*-alkyl nitriles and *n*-fatty aldehydes can be detected in Fractions 1 to 3, and high-polar compounds including *n*-alcohols, sterols, monoacylglycerides and fatty acids can be detected in Fractions 4 and 5.
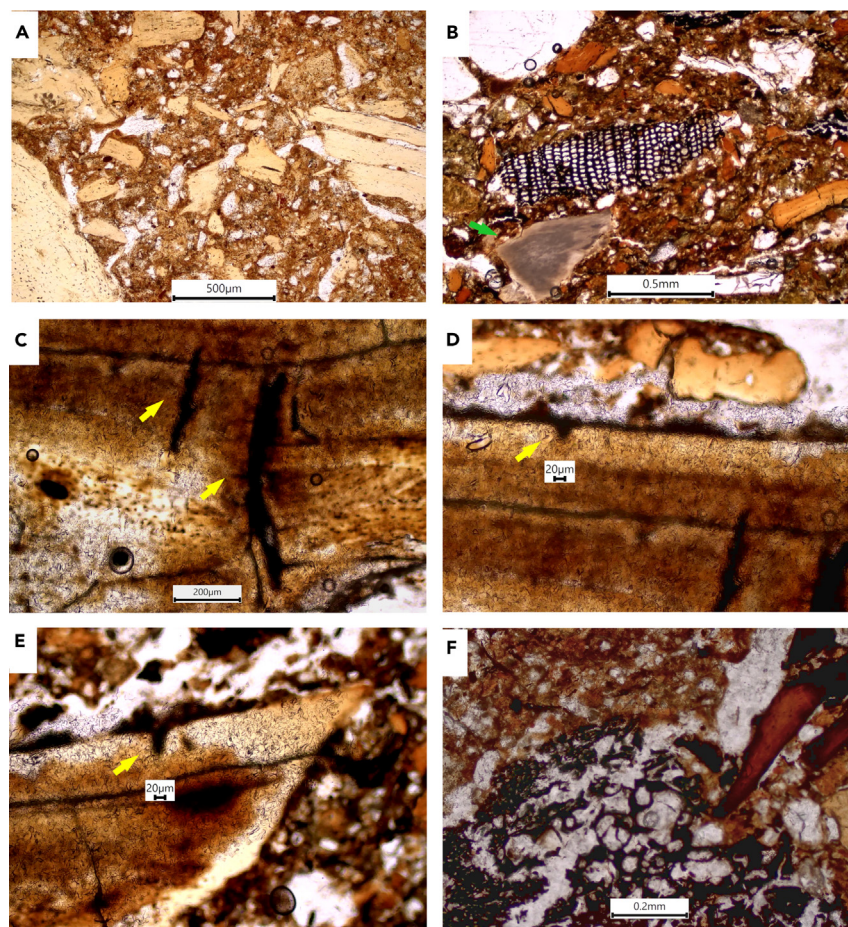
Figure 6. Different microscopic views of the Level N deposit in sample AX-18-1

(A) Concentration of unburned, subangular, sand-sized bone fragments in Facies N3 (PPL).

(B) Charcoal fragment and calcined bone fragment (green arrow) amongst other burned sand-sized burned bone (orange colored), PPL.

(C) Burned bone fragment from Facies N2 showing two parallel cut-marks on its surface (yellow arrows); PPL.

(D) Same bone fragment as in C, showing the cross-section of another cut-mark (yellow arrow); PPL.

(E) A different burned bone fragment from Facies N2 showing a cut-mark's cross-section (yellow arrow); PPL.

(F) Vesicular char fragment and a burned bone fragment (reddish-brown) in Facies N2.

The lipid biomarker composition of AX-18-1 profile consists of n-alkanes ranging from nC_{21} to nC_{33} (0.1 and 2.3 µg·gds^{-1}) with an odd-to-even preference and a unimodal distribution centered at nC_{31}, even-long chain n-alcohols ranging from nC_{26} to nC_{30} (0.03–0.16 µg·gds^{-1}) and peaking at nC_{26}, and even-short-chain fatty acids ($nC_{12:0}$ to $nC_{18:0}$) (0.10–0.50 µg·gds^{-1}), maximizing in $C_{16:0}$ and $C_{18:0}$. The AX-18-2 profile shows a similar lipid biomarker composition but with a different concentration and a few new compounds. The AX-18-2 lipid biomarker profile consists of n-alkanes ranging from nC_{15} to nC_{33} (6.0 and 8.3 µg·gds^{-1}) with an odd carbon number predominance and a unimodal distribution centered at nC_{31}, even long chain n-alcohols ranging from nC_{26} to nC_{30} (0.04–0.25 µg·gds^{-1}) and peaking at nC_{26}, and fatty acids ranging from nC_{12} to nC_{30} (0.23–7.45 µg·gds^{-1}) with an even-to-odd preference and maximizing in short-chain fatty acids ($C_{16:0}$ and $C_{18:0}$). In both profiles Facies N3 reported the high biomarker (n-alkane, n-alcohol and fatty acid) concentration (2.58 and 15.87 µg·gds^{-1} for AX-18-1 and AX-18-2, respectively) and Facies N1 reported the lowest values (0.69 and 6.08 µg·gds^{-1} for AX-18-1 and AX1-8-2, respectively) (Table 1). n-Alkane, n-alcohol and fatty acid compositions suggest a common terrestrial land plant wax source[23,36,37] in both profiles and no contribution from algae and/or bacteria, which are composed by short-chain n-alkanes (nC_{15}, nC_{17}, and nC_{19}).[38] However, the different n-alkane and fatty acid concentrations between the AX-18-1 profile (low concentrations), positioned more toward the inner cave and the AX-18-2 profile (high concentrations), positioned more toward the entrance of the cave, could suggest different degrees of preservation and/or organic matter accumulation.

To evaluate the degree of degradation of the sedimentary organic matter we used the carbon preference index (CPI)[39] of nC_{21}–nC_{33} homologues, the Average Chain Length (ACL)[40] of nC_{21}–nC_{33} homologues and long-chain n-alkane ratios[41] [LARs: $nC_{27}/(nC_{27}+nC_{31})$, $nC_{29}/(nC_{31}+nC_{29})$, $nC_{27}/(nC_{27}+nC_{29})$]. The CPI values in the AX-18-1 and AX-18-2 ranged from 2.4 to 4.5 and from 3.8 to 5.1, respectively,
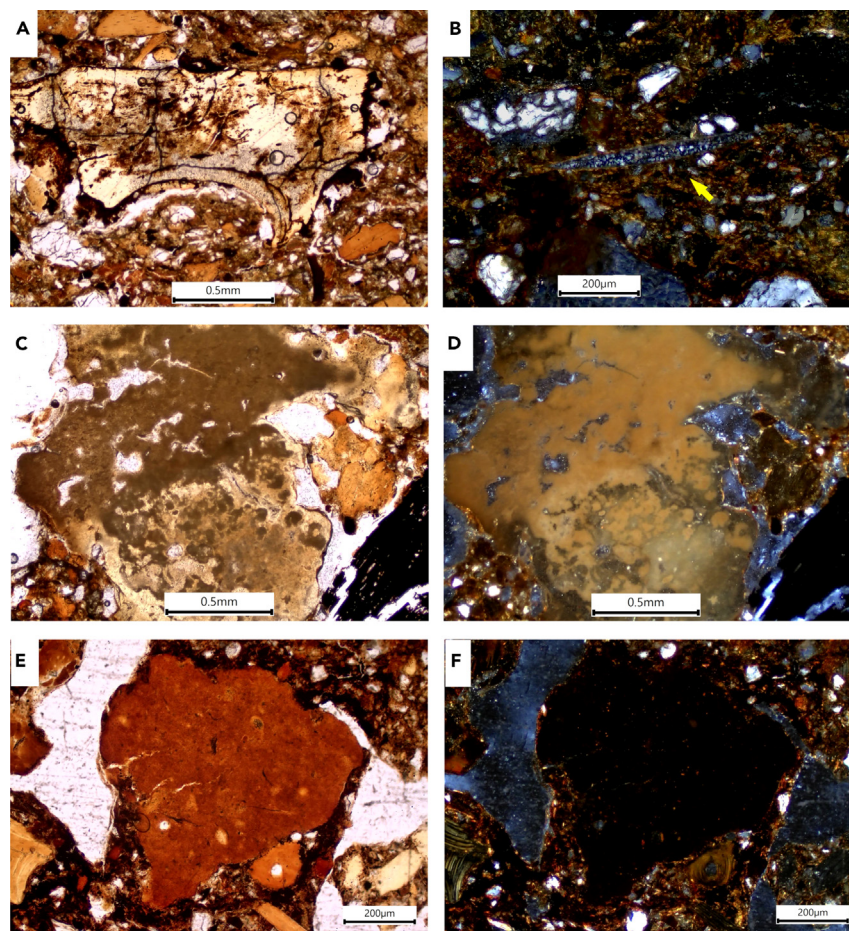
Figure 7. Different microscopic views of the Facies N2 deposit in sample AX-18-1

(A) Iron-stained bone fragment; PPL.

(B) A very thin flint flake viewed in XPL (yellow arrow). The white-gray grains are quartz sand.

(C) Omnivore or carnivore coprolite (PPL).

(D) Same as at left but in XPL.

(E) Burned omnivore or carnivore coprolite (PPL).

(F) Same as at left but in XPL.

and the ACL values varied from 27.7 to 29.1 and from 28.3 to 28.7, respectively. LARs values were similar throughout the sequence (Table 1). Among the different facies, N2 reported the highest CPI and ACL values in AX-18-1 whereas in AX-18-2, N2 reached the lowest values, with 1–2 units of difference within facies. Given that the CPI values from both profiles are higher than 1 there is no evidence of bacterial contribution or recycled organic matter,[38] corroborating the good states of organic matter preservation and the input of terrestrial land plants. Moreover, the ACL and LARs remains constant, suggesting input from the same natural source. Although in most grasses and herbs the n-alkane nC_{31} or nC_{33} dominate, whereas nC_{27} and nC_{29} are the n-alkane dominants in leaves from most trees and shrubs,[23,42,43] we cannot rule out the contribution of n-alkane nC_{31} from tree species (leaves).[23,43–45] In contrast to widely lipid biomarker references in leaves samples,[23,43–45] references of n-alkane composition in woody taxa is limited and only a few studies report dominance of mid and long-chain n-alkanes in fresh and charred (at low temperatures) woody taxa.[16,18,22] Neither polycyclic aromatic hydrocarbons (PAHs) nor n-ketones were detected in any profile which could help us to distinguish between angiosperms or gymnosperm plant contributions. However, low concentrations of diterpenoid dehydroabietic acid (m/z: 239, 357, 359) were detected in AX-18-2 Facies N2 (0.015 μg·gds^{-1}) and N3 (0.005 μg·gds^{-1}) which could suggest any contribution from conifers.[46] The absence of n-alkyl nitriles also suggest that if there was combustion, it was performed at low temperatures (<350°C), not high enough to produce n-alkyl nitriles.[13,47,48] This is consistent with the predominance of long-chain odd n-alkanes[13,23] and the absence of low CPI (~1) and low ACL (<24) values, indicative of combustion temperatures $\geq$300°C[21–23]

We detected two monoacylglycerides (MAGs), namely monopalmitin (0.01–0.83 μg gds^{-1}) and monostearin (0.01–0.03 μg·gds^{-1}) in AX-18-1 (Facies N1, N2 and N3), with the highest concentration in N2 in addition to glycerol (0.299 μg·gds^{-1}). No monoacylglycerides were detected in AX-18-2, only glycerol (0.749 μg·gds^{-1}) in Facies N2 and long-chain n-fatty aldehydes (tetracosanal) in N1 (0.10 μg.gds^{-1}), N2 and N3

Figure 8. Micromorphological sample AX-18-1 and Facies of Level N.

(0.03 µg·gds^{-1}) (Table 1). The fact that MAGs, glycerol and fatty acids were found in AX-18-1 points to the hydrolytic degradation of the acyl groups[49,50] since triacylglycerols are broken down to diacylglycerols, MAGs and finally, free fatty acids and glycerol.[50] The absence of MAGs in AX-18-2 and the presence of fatty acids and glycerol (Facies N2) in higher concentrations than in AX-18-1 suggest an advanced or final stage of the hydrolytic degradation of the acyl groups relative to AX-18-1.

Because of the incomplete hydrolysis of all acylglycerols in AX-18-1 and their potential isotopic effects on $\delta^{13}C$ values for fatty acids,[51] compound-specific stable isotope analysis ($\delta^{13}C_{16:0}$ and $\delta^{13}C_{18:0}$) were performed in AX-18-2 for fingerprint identification in this complex mixture. We used $\delta^{13}C_{-Fatty\ acids}$ to identify organic matter sources. $\delta^{13}C_{-Fatty\ acids}$ ($\delta^{13}C_{16:0}$ and $\delta^{13}C_{18:0}$) have great potential for tracing different types of animal fats[9,12,17,49,52,53] as well as plant oils[13,16,51,54,55] in archaeological residues. The carbon isotopic signatures of palmitic ($C_{16:0}$) and stearic ($C_{18:0}$) acids in AX-18-2 varied from −26.6‰ to −26.1‰ and from −25.4‰ to −22.7‰, respectively (Table 2). Our results were compared with $\delta^{13}C_{16:0}$ and $\delta^{13}C_{18:0}$ from modern plants tissues (leaves and wood) charred at low combustion temperatures (<300°C)[13,55] and modern animal fats.[52,53,56] These modern $\delta^{13}C$ values of the $C_{16:0}$ and $C_{18:0}$ fatty acids were corrected for variation in atmospheric $^{13}CO_2$ associated with the ^{13}C Suess effect by 1.9‰, assuming a pre-industrial $\delta^{13}C_{atm}$ value of −6.4‰[57] and the $\delta^{13}C_{atm}$ value at the time of sampling (−8.3‰)[58] to match archaeological $\delta^{13}C$ values.

The mean $\delta^{13}C$ values obtained from the sedimentary organic matter in Level N (−26.7‰ ± 0.6 and −24.3‰ ± 1.2) are more enriched than the fresh and dead charred leaves by 9‰ (n = 10, Hackberry and Pine),[13,55] and by 4‰ in fresh charred branches (n = 6, Hackberry and Pine)[13,55] for the $C_{16:0}$ and $C_{18:0}$ fatty acids, and by 1.7‰ and 1.3‰ for the $C_{16:0}$ and $C_{18:0}$ fatty acid respectively in dead charred branches (n = 3, Pine).[13,55] The latter has almost identical $\delta^{13}C$ than the organic matter from Level N suggesting dead-woody and charred tissues in the fine organic combustion residues; this is especially marked in Facies N2 (Figure 9A). On the other hand, we compare our $\delta^{13}C$ values with modern almost European reference fats[52,53,56] after applying $^{13}CO_2$ atmospheric correction, and are in agreement with fats from non-ruminant animals (Figure 9A). In Level N, 75% of the macrofaunal remains are from ruminants (deer, *Cervus*) whereas non-ruminant remains represent <5% (Equus, and only one macrofaunal remains of wild boar).[25] The mean $\delta^{13}C$ values for deer and Level N differ by 1‰–4‰ and 7‰-5‰, for horse and Level N by 3‰ and 5‰ and for wild boar and Level N by 1‰ and 3‰, in the $C_{16:0}$ and $C_{18:0}$ fatty acids respectively (Figure 9B). While the isotopic values for deer[52,53] and wild boar[56] are derived from wild species and could reflect diets that resemble those of Paleolithic species, the values for horses[53] pertain to domestic species and therefore, may not provide a representative indication of Paleolithic wild horses. There is a differentiation in $\delta^{13}C$ values between from Facies N1 (grayish-brown, clayey with charcoal and bone fragments) and Facies N2 (dark brown, clayey with frequent bone fragments and charcoal). The $\delta^{13}C$ values of organic residues found in Facies N1 and N3 (light brown, clayey with bone fragments and charcoal) may indicate a higher non-ruminant fat content compared to Facies N2. Despite the fact that 75% of the animal remains in Level N are deer, the fatty acids from Facies N1 are enriched in ^{13}C compared to modern deer fats from Poland[52] and the UK[53] (Figure 9B). Isotopic variability can result from different environmental and dietary conditions. On the other hand, Facies N2 reported a ^{13}C-enrichment ($C_{18:0}$) by 3‰ relative to N1 and N3 and may reflect more dead-woody and charred tissues in the fine organic combustion residues (Figure 9), suggesting dead wood gathering strategies by Neanderthal groups, tentatively related to conifer species (low dehydroabietic acid concentrations), although probably not the most abundant component. Deciduous woodland (*Alnus*, *Quercus robur* type, *Corylus*, *Betula*, and *Carpinus*) with significant proportions of *Fagus* were dominant during the early glacial period (MIS 5c) in the northwestern Iberian based on pollen data from the Area Longa sequence,[59] in contrast to the vegetation of central and southern Iberia (pollen typical of gymnosperms, Mediterranean or steppe).[59] Since conifers appear to have been very limited in the immediate vicinity at the Axlor site we do not discharge the use of other dead thermomediterranean woody taxa as fuel.[60,61] This is in agreement with the regionally formation of a mixed temperate forest[59,62,63] and the dominance of red deer in the faunal assemblage,[25] a key indicator of deciduous and mixed woodland ecosystems.

Conclusions

Our micromorphological and biomarker data indicates that Level N and base of Level M were formed under wet conditions during which recurrent human occupation took place. Level N at the sampled area along the West profile shows evidence of recurrent human occupation associated with butchery, flint knapping or tool use, and fire-making activities in close proximity to the sampled area. Evidence of trampling throughout Level N indicates *in situ* human occupation surfaces at the samples spots. No microscopic evidence of *in situ* combustion was identified.[2] Instead, the residues are possibly representative of hearth rake-out.[35] The lipid biomarker composition suggests low combustion temperatures, input of terrestrial land plants and good states of organic matter preservation. We observed a laterally hydrolytic degradation, with a more rapidly hydrolyzed AX-18-2 profile, positioned more toward the entrance of the cave, and slowly hydrolyzed AX-18-1 profile,

Table 1. Lipid biomarker concentrations obtained from Level N (Axlor)

Sampling Site West profile	AX-18-2			AX-18-1		
Facies description	N1-Grayish-brown, clayey with charcoal and bone fragments	N2-Dark brown, clayey with frequent bone fragments and charcoal	N3-Light brown, clayey with bone fragments and charcoal	N1-Grayish-brown, clayey with charcoal and bone fragments	N2-Dark brown, clayey with frequent bone fragments and charcoal	N3-Light brown, clayey with bone fragments and charcoal
Code sample	AX-18-2-N1	AX-18-2-N2	AX-18-2-N3	AX-18-1-N1	AX-18-1-N2	AX-18-1-N3
n-alkane concentration (nC_{21}-nC_{33}) ($\mu g \cdot gds^{-1}$)	6.05	6.46	8.35	0.14	0.79	2.24
n-alkane concentration (nC_{8}-nC_{19}) ($\mu g \cdot gds^{-1}$)	0.24	0.24	0.27	0.00	0.00	0.00
n-alkane concentration (nC_{20}-nC_{26}) ($\mu g \cdot gds^{-1}$)	1.34	1.81	1.93	0.06	0.18	0.78
n-alkane concentration (nC_{27}-nC_{33}) ($\mu g \cdot gds^{-1}$)	4.83	4.80	6.58	0.08	0.61	1.46
$nC_{27}/nC_{31}+nC_{27}$	0.28	0.29	0.26	0.22	0.19	0.28
$nC_{29}/nC_{31}+nC_{29}$	0.52	0.50	0.53	0.69	0.63	0.59
$nC_{27}/nC_{27}+nC_{29}$	0.29	0.29	0.28	0.39	0.29	0.36
CPI[39] (nC_{21}-nC_{33})	5.06	3.85	4.79	3.94	4.50	2.45
ACL[40] (nC_{21}-nC_{33})	28.72	28.29	28.67	27.66	29.10	27.98
n-fatty aldehydes concentration (nC_{24}) ($\mu g \cdot gds^{-1}$)	0.10	0.03	0.03	ND	ND	ND
n-alcohols concentration (nC_{22}-nC_{30}) ($\mu g \cdot gds^{-1}$)	ND	0.25	0.04	0.06	0.16	0.03
Glycerol, 3TMS ($\mu g.gds^{-1}$)	ND	ND	ND	ND	0.299	ND
2-Palmitoylglycerol, 2TMS ($\mu g \cdot gds^{-1}$)	ND	ND	ND	0.001	0.007	ND
1-Monopalmitin, 2TMS ($\mu g \cdot gds^{-1}$)	ND	ND	ND	0.010	0.083	ND
2-Monostearin, 2TMS ($\mu g \cdot gds^{-1}$)	ND	ND	ND	ND	0.003	0.003
Glycerol monostearate, 2TMS ($\mu g.gds^{-1}$)	ND	ND	ND	0.009	0.038	0.004
Dehydroabietic acid TMS ($\mu g \cdot gds^{-1}$)	ND	0.015	0.005	ND	ND	ND
Fatty acid concentration (nC_{12}-nC_{33}) ($\mu g \cdot gds^{-1}$)	0.23	1.88	7.45	0.50	0.10	0.31
Fatty acid concentration (nC_{12}, nC_{14}, nC_{16}, nC_{18}) ($\mu g \cdot gds^{-1}$)	0.23	0.08	2.51	0.50	0.10	0.31
Fatty acid concentration (nC_{20}, nC_{22}, nC_{24}) ($\mu g \cdot gds^{-1}$)	0.00	0.02	0.92	ND	ND	ND
Fatty acid concentration (nC_{26}, nC_{28}, nC_{30}) ($\mu g \cdot gds^{-1}$)	0.00	1.78	4.02	ND	ND	ND

ND no detected

Table 2. Carbon isotope values of $C_{16:0}$ and $C_{18:0}$ fatty acids plus standard deviation and the difference in the $\delta^{13}C$ isotope values ($\Delta^{13}C$) of the individual $C_{16:0}$ and $C_{18:0}$ fatty acids obtained from Leven N (Axlor)

Sampling site West profile	AX-18-2		
Facies description	N1-Grayish-brown, clayey with charcoal and bone fragments	N2-Dark brown, clayey with frequent bone fragments and charcoal	N3-Light brown, clayey with bone fragments and charcoal
Code sample	AX-18-2-N1	AX-18-2-N2	AX-18-2-N3
$\delta^{13}C_{16:0}$ (‰) VPDB $\pm\sigma$	−26.1 ± 0.4	−26.6 ± 0.2	−26.6 ± 0.3
$\delta^{13}C_{18:0}$ (‰) VPDB $\pm\sigma$	−25.4 ± 0.1	−22.7 ± 0.3	−24.8 ± 0.2
$\Delta^{13}C$ ($\delta^{13}C_{18:0}$ - $\delta^{13}C_{16:0}$)	0.7	3.9	1.8

positioned more toward the inner cave. Human occupation was possibly more intense during the formation of Facies N2, the black layer, with a mixture of fine organic combustion residues from charred dead wood and non-ruminant fats. Our data also suggest the use of dead wood by Neanderthal groups, a common hunter-gatherer practice.[4] Level M contains abundant fragmented unburned bone and no evidence of knapping, combustion activity or trampling at the sampled area. The Level M-N sequence was later affected by mass movement causing slight microscopic physical disturbance such as in solifluction and tentatively could be correlated with MIS5c (Level N and base of Level M).

Limitations of the study

A limitation of the study is that the number of samples in Level N (n = 3) is low for statistical tests. On the other hand the reference database of modern plant oils (fresh and charred tissues) as well as the references from iberian and european animal fats (fatty acid composition of fat in animals depends on the fat composition of the diet) are limited, particularly in the case of plant oils. However, the discrimination observed
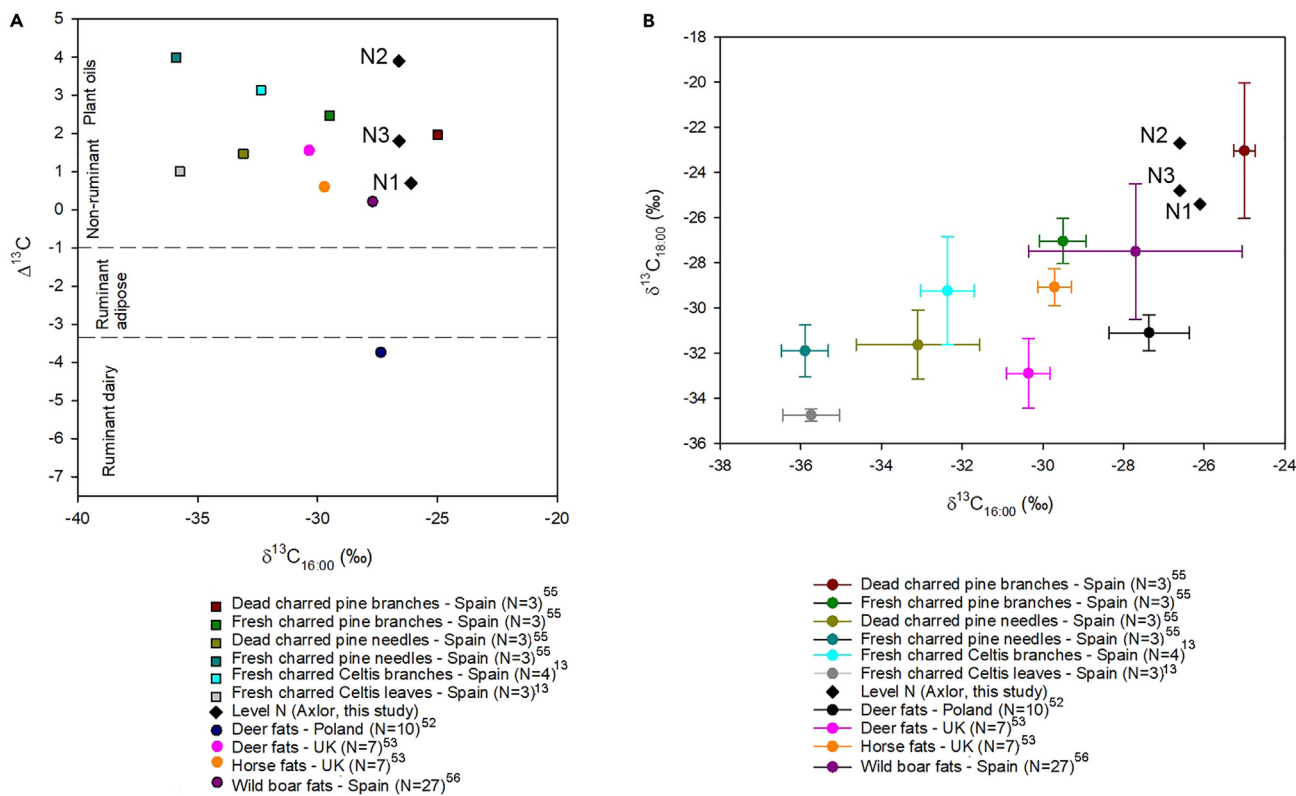

Figure 9. Stable carbon isotope measurements of C16:0 and C18:0 fatty acids obtained from Level N sediment samples against ranges of reference fats and oils

(A) The $\Delta^{13}C$ ($\delta^{13}C_{18:0}$ - $\delta^{13}C_{16:0}$) values plotted against the $\delta^{13}C_{16:0}$ and (B) plot of the $\delta^{13}C$ values of the fatty acids $C_{16:0}$ and $C_{18:0}$ from corrected modern animal fats (mean values)[52,53,56] and charred plant tissues (mean values)[13,55] references compared with the data obtained for Level N (N3, N2 and N1).

between Facies N2 and N1 and good matching with previous $\delta^{13}C$ values of the fatty acids $C_{16:0}$ and $C_{18:0}$ from dead-woody oils and non-ruminant fats suggest that compound-specific stable isotope analysis ($\delta^{13}C_{Faty\ acids}$) allow differentiation between animal fats and plant oils and the state of degradation of wood.

STAR★METHODS

Detailed methods are provided in the online version of this paper and include the following:

- KEY RESOURCES TABLE
- RESOURCE AVAILABILITY
  - Lead contact
  - Materials availability
  - Data and code availability
- EXPERIMENTAL MODEL AND SUBJECT DETAILS
- METHOD DETAILS
  - Micromorphology sample processing and analysis
  - Lipid biomarker extraction and separation
  - Instrumental analyses
  - Identification and quantification

AUTHOR CONTRIBUTIONS

M.J.E.: conceptualization, methodology, investigation, validation, formal analysis, and writing – original draft preparation, C.M.: conceptualization, methodology, investigation, formal analysis, resources, writing – original draft preparation, and funding acquisition, A.V.H.H. methodology, validation, formal analysis, data curation, and writing – review and editing, J.G.U: resources and writing – review and editing, L-T.L.F.: resources and writing – review and editing.

DECLARATION OF INTERESTS

The authors declare that they have no known competing financial interests or personal relationships that could have appeared to influence the work reported in this article.

REFERENCES

1. Aldeias, V. (2017). Experimental Approaches to Archaeological Fire Features and Their Behavioral Relevance. Curr. Anthropol. *58*, S191–S205.

2. Mallol, C., Mentzer, S.M., and Miller, C.E. (2017). Combustion features. Archaeological soil and sediment micromorphology. In Archaeological Soil and Sediment Micromorphology, C. Nicosia and G. Stoops, eds. (John Wiley & Sons Ltd), pp. 299–330.

3. Roebroeks, W., and Villa, P. (2011). On the earliest evidence for habitual use of fire in Europe. Proc. Natl. Acad. Sci. USA *108*, 5209–5214.

4. Allué, E., Mallol, C., Aldeias, V., Burguet-Coca, A., Cabanes, D., Carrancho, A., and Vaquero, M. (2022). Fire among Neanderthals. In Updating Neanderthals, F. Romagnoli, F. Rivals, and S. Benazzi, eds. (Academic Press), pp. 227–249.

5. Murphree, W.C., and Aldeias, V. (2022). The evolution of pyrotechnology in the Upper Palaeolithic of Europe. Archaeol. Anthropol. Sci. *14*, 202.

6. Aldeias, V., Mallol, C., and Goldberg, P. (2021). From Fire to Behavior. Documenting Archaeological Fire Evidence in the Field. In Préhistoireet Protohistoire de l'Ouest de la France: Nouvelles perspectives en hommage à Jean-Laurent Monnier, pp. 41–77.

7. Weiner, S. (2010). Microarchaeology: Beyond the Visible Archaeological Record (Cambridge University Press).

8. Mentzer, S.M. (2014). Microarchaeological approaches to the identification and interpretation of combustion features in prehistoric archaeological sites. J. Archaeol. Method Theor *21*, 616–668.

9. March, R. (2013). Searching for the functions of fire structures in Eynan (Mallaha) and their formation processes: a geochemical approach. In Natufian Foragers in the Levant Terminal Pleistocene - Social Changes in Western Asia. International Monographs in Prehistory Archaeological Series 19(17), O. Bar-Yosef and F.R. Valla, eds., pp. 227–284.

10. March, R.J., Whallon, R., and Morley, M.W. (2018). Studying neanderthal fire structures from Crvena Stijena. In Crvena Stijena in cultural and ecological context: Multidisciplinary archaeological research in Montenegro, R. Wallon, ed. (Montenegrin Academy of Sciences and Arts: National Museum of Montenegro), pp. 340–449.

11. Mallol, C., Hernández, C.M., Cabanes, D., Sistiaga, A., Machado, J., Rodríguez, Á., Pérez, L., and Galván, B. (2013). The black layer of Middle Palaeolithic combustion structures. Interpretation and archaeostratigraphic implications. J. Archaeol. Sci. *40*, 2515–2537.

12. Choy, K., Potter, B.A., McKinney, H.J., Reuther, J.D., Wang, S.W., and Wooller, M.J. (2016). Chemical profiling of ancient hearths reveals recurrent salmon use in Ice Age Beringia. Proc. Natl. Acad. Sci. USA *113*, 9757–9762.

13. Jambrina-Enríquez, M., Herrera-Herrera, A.V., Rodríguez de Vera, C., Leierer, L., Connolly, R., and Mallol, C. (2019). n-Alkyl nitriles and compound-specific carbon isotope analysis of lipid combustion residues from Neanderthal and experimental hearths: identifying sources of organic compounds and combustion temperatures. Quat. Sci. Rev. *222*, 105899.

14. Jambrina-Enríquez, M., Mallol, C., Tostevin, G., Monnier, G., Pajović, G., Borovinić, N., and Baković, M. (2022). Hydroclimate reconstruction through MIS 3 in the Middle Paleolithic site of Crvena Stijena (Montenegro) based on hydrogen-isotopic composition of sedimentary n-alkanes. Quat. Sci. Rev. *295*, 107771.

15. Leierer, L., Jambrina-Enríquez, M., Herrera-Herrera, A.V., Connolly, R., Hernández, C.M., Galván, B., and Mallol, C. (2019). Insights into the timing, intensity and natural setting of Neanderthal occupation from the geoarchaeological study of combustion structures: A micromorphological and biomarker investigation of El Salt, unit Xb, Alcoy, Spain. PLoS One *14*, e0214955.

16. Tomé, L., Jambrina-Enríquez, M., Égüez, N., Herrera-Herrera, A.V., Davara, J., Marrero Salas, E., Arnay de la Rosa, M., and Mallol, C. (2022). Fuel sources, natural vegetation and subsistence at a high-altitude aboriginal settlement in Tenerife, Canary Islands: Microcontextual geoarchaeological data from Roques de García Rockshelter. Archaeol. Anthropol. Sci. *14*, 195.

17. Buonasera, T., Herrera-Herrera, A.V., and Mallol, C. (2019). Experimentally derived sedimentary, molecular, and isotopic characteristics of bone-fueled hearths. J. Archaeol. Method Theor *26*, 1327–1375.

18. Jambrina-Enríquez, M., Herrera-Herrera, A.V., and Mallol, C. (2018). Wax lipids in fresh and charred anatomical parts of the Celtis australis tree: Insights on paleofire interpretation. Org. Geochem. *122*, 147–160.

19. Connolly, R., Jambrina-Enríquez, M., Herrera-Herrera, A.V., and &Mallol, C. (2021). Investigating hydrogen isotope variation during heating of n-Alkanes under limited oxygen conditions: implications for palaeoclimate reconstruction in archaeological settings. Molecules *26*, 1830.

20. Braadbaart, F., and Poole, I. (2008). Morphological, chemical and physical changes during charcoalification of wood and its relevance to archaeological contexts. J. Archaeol. Sci. *35*, 2434–2445.

21. Wiesenberg, G., Lehndorff, E., and Schwark, L. (2009). Thermal degradation of rye and maize straw: lipid pattern changes as a function of temperature. Org. Geochem. *40*, 167–174.

22. Knicker, H., Hilscher, A., De la Rosa, J., González-Pérez, J., and González-Vila, F. (2013). Modification of biomarkers in pyrogenic organic matter during the initial phase of charcoal biodegradation in soils. Geoderma *197–198*, 43–50.

23. Diefendorf, A.F., Sberna, D.T., and Taylor, D.W. (2015). Effect of thermal maturation on plant-derived terpenoids and leaf wax n-alkyl components. Org. Geochem. *89–90*, 61–70.

24. Aldeias, V., Dibble, H.L., Sandgathe, D., Goldberg, P., and McPherron, S.J. (2016). How heat alters underlying deposits and implications for archaeological fire features: a controlled experiment. J. Archaeol. Sci. *67*, 64–79.

25. Castaños, P. (2005). Revisión actualizada de las faunas de macromamíferos del Würm antiguo en la Región Cantábrica. In Neandertales cantábricos, estado de la cuestión, R. Montes and J.A. Las heras, eds. (Museo Nacional y Centro de Investigación de Altamira), pp. 201–207.

26. Mozota, M. (2012). El hueso como materia prima: El utillaje óseo del final del Musteriense en el sector central del norte de la Península Ibérica, Tesis doctoral (Universidad de Cantabria).

27. Lazuen, T., and González Urquijo, J. (2020). El estudio de las formas de vida de las sociedades neandertales en el yacimiento de Axlor: las excavaciones de J.M. Barandiaran y el proyecto del siglo XXI. Anuario de Eusko Folklore *54*, 47–69.

28. González-Urquijo, J., Bailey, S.E., and Lazuen, T. (2021). Axlor'slevel IV human remains are convincingly Neanderthals: A reply to Gómez-Olivencia et al. Am. J. Phys. Anthropol. *1*, 6.

29. Gonzalez-Urquijo, J. (2005). Inventario de materiales arqueológicos depositados en el Museo Arqueológico, Etnográfico e Histórico vasco de Bilbao, yacimiento de Axlor, excavaciones de J.M. de Barandiarán (Culture Department, Basque Government).

30. Demuro, M., Arnold, L.J., González-Urquijo, J., Lazuen, T., and Frochoso, M. (2023). Chronological constraint of Neanderthal cultural and environmental changes in southwestern Europe: MIS 5–MIS 3 dating of the Axlor site (Biscay, Spain). J. Quat. Sci. *38*, 891–920.

31. González-Urquijo, J., Ibáñez, J.J., Ríos, J., and Bourguignon, L. (2006). Aportes de las nuevas excavaciones en Axlor sobre el final del Paleolítico Medio. In En el centenario de la cueva de El Castillo: el ocaso de los neandertales Cabrera, V. Bernaldo De Quirós and F. Maíllo, eds. (UNED), pp. 269–290.

32. Villagran, X.S., Huisman, D.J., Mentzer, S.M., Miller, C.E., and Jans, M.M. (2017). Bone and other skeletal tissues. In Archaeological Soil and Sediment Micromorphology, C. Nicosia and G. Stoops, eds. (John Wiley & Sons Ltd), pp. 9–38.

33. Lambrecht, G., and Mallol, C. (2020). Autofluorescence of experimentally heated bone: potential archaeological applications and relevance for estimating degree of burning. J. Archaeol. Sci. Rep. *31*, 102333.

34. Lambrecht, G., Rodríguez de Vera, C., Jambrina-Enríquez, M., Crevecoeur, I., Gonzalez-Urquijo, J., Lazuen, T., and Mallol, C. (2021). Characterisation of charred organic matter in micromorphological thin sections by means of Raman spectroscopy. Archaeol Anthropol Sci *13*, 1–15.

35. Miller, C.E., Conard, N.J., Goldberg, P., and Berna, F. (2010). Dumping, sweeping and trampling: experimental micromorphological analysis of anthropogenically modified combustion features. Palethnologie *2*, 25–37.

36. Eglinton, T.I., and Eglinton, G. (2008). Molecular proxies for paleoclimatology. Earth Planet Sci. Lett. *275*, 1–16.

37. Diefendorf, A.F., and Freimuth, E.J. (2017). Extracting the most from terrestrial plant-derived n-alkyl lipids and their carbon isotopes from the sedimentary record: A review. Org. Geochem. *103*, 1–21.

38. Cranwell, P.A., Eglinton, G., and Robinson, N. (1987). Lipids of aquatic organisms as potential contributors to lacustrine sediments—II. Org. Geochem. *11*, 513–527.

39. Bray, E.E., and Evans, E.D. (1961). Distribution of n-paraffins as a clue to recognition of source beds. Geochem. Cosmochim. Acta *22*, 2–15.

40. Poynter, J.G., Farrimond, P., Robinson, N., and Eglinton, G. (1989). Aeolian-Derived Higher Plant Lipids in the Marine Sedimentary Record: Links with Palaeoclimate. In Paleoclimatology and Paleometeorology: Modern and Past Patterns of Global Atmospheric Transport, M. Leinen and M. Sarnthein, eds. (Springer), pp. 435–462. NATO ASI Series, vol 282.

41. Buggle, B., Wiesenberg, G.L., and Glaser, B. (2010). Is there a possibility to correct fossil n-alkane data for postsedimentary alteration effects? Appl. Geochem. *25*, 947–957.

42. Schwark, L., Zink, K., and Lechterbeck, J. (2002). Reconstruction of postglacial to early Holocene vegetation history in terrestrial Central Europe via cuticular lipid biomarkers and pollen records from lake sediments. Geology *30*, 463–466.

43. Bush, R.T., and McInerney, F.A. (2015). Influence of temperature and C4 abundance on n-alkane chain length distributions across the central USA. Org. Geochem. *79*, 65–73.

44. Dodd, R.S., and Poveda, M.M. (2003). Environmental gradients and population divergence contribute to variation in cuticular wax composition in Juniperus communis. Biochem. Systemat. Ecol. *31*, 1257–1270.

45. Suh, Y.J., and Diefendorf, A.F. (2018). Seasonal and canopy height variation in n-alkanes and their carbon isotopes in a temperate forest. Org. Geochem. *116*, 23–34.

46. Otto, A., and Wilde, V. (2001). Sesqui-di-and triterpenoids as chemosystematic markers in extant conifers—a review. Bot. Rev. *67*, 141–238.

47. Ishiwatarii, R., Sugawara, S., and Machihara, T. (1992). Long-chain aliphatic nitriles in pyrolysates of young kerogen: implications for the intermediates in petroleum hydrocarbon formation. Geochem. J. *26*, 137–146.

48. Rushdi, A.I., bin Abas, M.R., Didyk, B.M., and Didyk, B.M. (2003). Alkyl amides and nitriles as novel tracers for biomass burning. Environ. Sci. *37*, 16–21.

49. Dudd, S.N., Evershed, R.P., and Gibson, A.M. (1999). Evidence for varying patterns of exploitation of animal products in different prehistoric pottery traditions based on lipids preserved in surface and absorbed residues. J. Archaeol. Sci. *26*, 1473–1482.

50. Evershed, R.P., Dudd, S.N., Copley, M.S., and Mutherjee, A. (2002). Identification of animal fats via compound specific δ13C values of individual fatty acids: assessments of results for reference fats and lipid extracts of archaeological pottery vessels. Doc. Praeh. *29*, 73–96.

51. Steele, V.J., Stern, B., and Stott, A.W. (2010). Olive oil or lard?: Distinguishing plant oils from animal fats in the archeological record of the eastern Mediterranean using gas chromatography/combustion/isotope ratio mass spectrometry. Rapid Commun. Mass Spectrom. *24*, 3478–3484.

52. Craig, O.E., Allen, R.B., Thompson, A., Stevens, R.E., Steele, V.J., and Heron, C. (2012). Distinguishing wild ruminant lipids by

gas chromatography/combustion/isotope ratio mass spectrometry. Rapid Commun. Mass Spectrom. *26*, 2359–2364.

53. Dudd, S.N. (1999). Molecular and Isotopic Characterisation of Animal Fats in Archaeological Pottery (Doctoral dissertation, University of Bristol).

54. Spangenberg, J.E., Jacomet, S., and Schibler, J. (2006). Chemical analyses of organic residues in archaeological pottery from Arbon Bleiche 3, Switzerland–evidence for dairying in the late Neolithic. J. Archaeol. Sci. *33*, 1–13.

55. Jambrina-Enríquez, M., Rodríguez de Vera, C., Davara, J., Herrera-Herrera, A.V., and Mallol, C. (2023). Compound-specific carbon isotope analysis of short-chain fatty acids from Pine tissues: characterizing paleo-fire residues and plant exudates. Archaeol Anthropol Sci *15*, 114.

56. Tarifa-Mateo, N., Saña, M., Clop, X., Rosell-Melé, A., Camalich-Massieu, M.D., and Martín-Socas, D. (2023). Investigating livestock management in the early Neolithic archaeological site of Cabecicos Negros (Almería, Spain) from the organic residue analysis in pottery. Sci. Rep. 4797.5.

57. McCarroll, D., and Loader, N.J. (2004). Stable isotopes in tree rings. Quat. Sci. Rev. *23*, 771–801.

58. Keeling, R.F., Piper, S.C., Bollenbacher, A.F., and Walker, S.J. (2010). Monthly Atmospheric 13C/12C Isotopic Ratios for 11 SIO Stations (1977-2008) Trends: A Compendium of Data on Global Change. Carbon Dioxide Information Analysis Center (Oak Ridge National Laboratory, U.S. Department of Energy).

59. Gómez-Orellana, L., Ramil-Rego, P., and Muñoz Sobrino, C. (2007). The Würm in NW Iberia, a pollen record from Area Longa (Galicia). Quat. Res. *67*, 438–452.

60. Badal, E., Carrión, Y., Figueiral, I., and Rodríguez Ariza, M.O. (2013). Pinares y enebrales. El paisaje solutrense en Iberia Espacio, Tiempo y Forma. Serie I. Prehistoria y Arqueología 5, 259–271.

61. Carrión, J.S., Finlayson, C., Fernández, S., Finlayson, G., Allué, E., López-Sáez, J.A., Lopezgarcia, P., Gilromera, G., Bailey, G., Gonzalezsamperiz, P., and González-Sampériz, P. (2008). A coastal reservoir of biodiversity for Upper Pleistocene human populations: palaeoecological investigations in Gorham's Cave (Gibraltar) in the context of the Iberian Peninsula. Quat. Sci. Rev. *27*, 2118–2135.

62. Daniau, A.L., Goñi, M.F.S., and Duprat, J. (2009). Last glacial fire regime variability in western France inferred from microcharcoal preserved in core MD04-2845, Bay of Biscay. Quat. Res. *71*, 385–396.

63. Sánchez Goñi, M.F., Landais, A., Fletcher, W.J., Naughton, F., Desprat, S., and Duprat, J. (2008). Contrasting impacts of Dansgaard–Oeschger events over a western European latitudinal transect modulated by orbital parameters. Quat. Sci. Rev. *27*, 1136–1151.

64. Goodman, K.J., and Brenna, J.T. (1992). High sensitivity tracer detection using high-precision gas chromatography-combustion isotope ratio mass spectrometry and highly enriched [U-13C]-labelled precursors. Anal. Chem. *64*, 1088–1095.

STAR★METHODS

KEY RESOURCES TABLE

REAGENT or RESOURCE	SOURCE	IDENTIFIER
Chemicals, peptides, and recombinant proteins		
Dichloromethane Chromasolv® for HPLC grade, purity ≥99.8%	Honeywell	CAS75-09-2
Methanol Chromasolv® for HPLC grade and MeOH, purity ≥99.9%	Honeywell	CAS67-56-1
Hexane Chromasolv® for HPLC grade purity ≥97%	Honeywell	CAS110-54-3
Ethyl Acetate Chromasolv® for HPLC grade purity ≥97%	Honeywell	
5α-androstane purity ≥99.9%	Sigma-Aldrich	CAS438-22-2
5α-androstan-3β-ol, purity ≥99.9%	Sigma-Aldrich	CAS474-25-9
N,O-Bis(trimethylsilyl)trifluoroacetamide with trimethylchlorosilane (99%), contains 1% Trimethylchlorosidane	Sigma-Aldrich	CAS25561-30-2
Sulfuric acid, purity 95–97%	Honeywell	CAS7664-93-9
Pure quarz sand (50–70 mesh)	Honeywell	CAS14808-60-7
Silica (technical grade, pore size 60 Å, 70–230 mesh, 63–200 μm)	Supelco	CAS112-926-00-8
Methyl nonadecanoate (C19:0)	Supelco	CAS1731-94-8
Hexadecanoic acid d31 (C16:0-d31)	Supelco	CAS39756-30-4
FAME standard mixture ($C_{14:0}$ methyl ester to $C_{20:0}$ ethyl ester)	Arndt Schimmelmann Biogeochemical Laboratories	https://hcnisotopes.earth.indiana.edu/reference-materials/materials-descriptions/fatty-acid-esters.html
Milli-Q®	Millipore	CAS7732-18-5
PALATAL P4-01 STRAINER RESIN	TNK composites	Cat#UM1866
Styrene monomer	TNK composites	CAS100-42-5
Methyl Ethyl Ketone Peroxide (MEKP)	TNK composites	CA78-93-3
Software and algorithms		
MassHunter Workstation	Agilent Technologies	https://www.agilent.com/en/products/software-informatics/masshunter-suite/masshunter-quantitative-analysis
NIST Mass Spectra Database v.14	National Institute of Standards and Technology (NIST)	https://chemdata.nist.gov/
IsoDat 3.0 software	Thermo Scientific	https://www.thermofisher.com/es/es/home/technical-resources/software-downloads.html
SigmaPlot v 14.0	Systat software	https://systatsoftware.com/product/sigmaplot-v15-upgrade-from-v14/
Other		
Furnace TR240	Nabertherm GmbH	https://nabertherm.com/en/products/labor/ovens-and-forced-convection/ovens-electrically-heated CAT#
Ultrasonic USC 600th	VWR International	Cat#142-0090
Centrifuge Mega Star 1.6	VWT International)	Cat#521-26-59
Nitrogen evaporator (RapidVap® Vertex Evaporator)	Labconco	Cat#7320037
Nitrogen evaporator (24 positions N-EVAP)	Organomation Associates Inc.	Cat#11250
Nikon Eclipse E200 polarizing microscope	Nikon Instruments Inc.	https://www.microscope.healthcare.nikon.com/products/upright-microscopes/eclipse-e200

Continued

REAGENT or RESOURCE	SOURCE	IDENTIFIER
Olympus BX53 polarizing microscope	Olympus IMS	https://www.olympus-ims.com/en/microscope/bx53m/
GC-Agilent 7890B	Agilent	https://www.agilent.com/en/product/gas-chromatography/gc-systems/7890b-gc-system
MSD Agilent 5977A	Agilent	https://www.agilent.com/en/promotions/gc-gcms-resolve
Thermo Scientific Isotope Ratio Mass Spectrometer Delta V Advantage	Thermo Scientific	https://www.thermofisher.com/es/es/home/industrial/mass-spectrometry/isotope-ratio-mass-spectrometry-irms/gas-isotope-ratio-mass-spectrometry-irms.html
GC Trace1310	Thermo Scientific	Cat#PGA000010011
Conflo IV	Thermo Scientific	Cat#IQLAAEGAATFAETMAXB
GC Isolink II	Thermo Scientific	Cat#IQLAAEGAATFAETMATA

RESOURCE AVAILABILITY

Lead contact

Further information and requests should be directed to and will be fulfilled by the lead contact, Dr. Margarita Jambrina-Enríquez (mjambrin@ull.edu.es).

Materials availability

This study did not generate new materials.

Data and code availability

- All data associated with the publication are included in this article.
- This paper does not report original code.
- Other items: there are no other items associated with the publication. Any additional information required to reanalyse the data reported in this paper is available from the lead contact upon request.

EXPERIMENTAL MODEL AND SUBJECT DETAILS

Our study does not use experimental models.

METHOD DETAILS

Micromorphology sample processing and analysis

In the lab, the block was impregnated with a resin mixture, cut and mounted on glass, producing four 6 cm × 9 cm x 30 μm thin sections following the standard AMBILAB protocol.[15] The thin sections (AX-18-1a, -1b, -1c and -1d) were observed under plane polarized, cross polarized and blue light using a Nikon Eclipse E200 polarizing microscope and an Olympus BX53 polarizing microscope, using 2×, 4× and 10× objectives.

Microscopic observations are qualitative and words are used to refer to changes in relative proportions (rare, few, frequent, abundant). Lithology (color, texture, grain size and composition) was subjectively described, not quantified and is not an object of investigation in this study. Only evident physical properties indicative of depositional mechanisms such as good sorting, bedding or sharp lithological changes were recorded.

Lipid biomarker extraction and separation

Lipid biomarker extraction and separation were performed at the Archaeological Micromorphology and Biomarkers (AMBILAB) (University of La Laguna, Spain) following the protocol described by Jambrina-Enriquez et al.[13,14,18] Prior to total lipid extraction, 2 g of each sediment sample was oven-dried at 60°C for 48 h and homogenized with an agate mortar. Soluble organic content was extracted by ultrasonic extraction (3 cycles × 30 min) with 20 mL of dichloromethane/methanol (DCM:MeOH, 9:1, v/v) at controlled temperatures (≤30°C), followed by centrifugation (3 cycles at 4700 rpm × 10 min).[13,14,18] The centrifuged solvent was filtered through annealed pyrolized glass wool (previously calcined at 450°C during 10 h) and evaporated under N_2 flow in a Nitrogen evaporator at 40°C.

The total lipid extract (TLE) was separated using solid phase extraction (SPE) into five fractions of different polarity on a 2 mL SPE column filled with pyrolized glass wool, 0.1 g pyrolized pure quartz sand and 1 g of pyrolized activated silica. The solid phase columns were preconditioned with 1.5 mL of hexane (1 portion of dead volume, DV). Fraction 1 (F1: *n*-alkanes) eluted with 560 μL in hexane (3/8 of DV), fraction 2 (F2: aromatics) with 3 mL in hexane:DCM (8:2, v/v) (2DV), fraction 3 (F3: ketones) with 3 mL in DCM (2DV), fraction 4 (F4: *n*-alcohols) with 3 mL in DCM/ethyl acetate (1:1, v/v) (2DV) and fraction 5 (F5: acids and diols) with 3 mL in EtOAc (2DV). The eluent was evaporated under a nitrogen flow in an Organomation evaporator.

After addition of 1 μL of internal standard (IS) 5α-androstane (400 mg/L in DCM) in F1, F2 and F3, the residue was re-dissolved in 50 μL of DCM for injection into the GC-MS system. 1/3 of F4 was derivatized by silylation procedure by heating the DCM dissolved fraction with the IS (1 μL of 5α-androstan-3β-ol, 400 mg/L in DCM) at 80°C for 1 h with the addition of 100 μL of N,O-Bis(trimethylsilyl)trifluoroacetamide (BSTFA) and trimethylchlorosilane (TCMS) (99:1, v/v). The fraction was then evaporated under a N_2 flow in an Organomation evaporator and reconstituted with 50 μL of DCM for injection into the GC-MS system. 1/3 of F5 was derivatized by methylation procedure to convert the free fatty acids (FAs) to their respective methyl-esters (FAMEs) and determine their carbon isotope ratios. After addition of 8 mg/L of ISs (methyl C19:0 and C16:0-d31), FAs were derivatized by adding 5 mL of MeOH and 400 μL of de H_2SO_4, heated at 70°C for 4 h in a RapidVap Vertex Evaporator, and posteriorly neutralized with a sodium bicarbonate saturated solution. FAMEs were extracted using 3 mL of hexane (3 cycles), evaporated under a N_2 flow in RapidVap Vertex Evaporator, and reconstituted with 50 μL of DCM for injection into the GC-MS system.

Instrumental analyses

Gas chromatography-mass spectrometry and compound-specific stable isotope analysis were performed at the Archaeological Micromorphology and Biomarkers (AMBILAB) (University of La Laguna, Spain) following the protocol described by Jambrina-Enriquez et al.[13,14] All the fractions were analyzed and quantified by gas chromatography with a coupled mass-selective detector (GC-Agilent 7890B attached to an MSD Agilent 5977A) equipped with an HP-5MS capillary column (30 m length x 0.25 mm i.d., 0.25 μm film thickness). The initial temperature for the GC was programmed at 70°C for 2 min followed by a heating rate of 12°C/min to 140°C and, finally, it reached a temperature of 320°C at a rate of 3°C/min and held for 15 min. The multimode injector was held at a split ratio of 5:1 at an initial temperature of 70°C for 0.85 min and heated to 300°C at a programmed rate of 720°C/min. All measurements were done in duplicate.

Carbon isotope analyses of the fatty acids $C_{16:0}$ and $C_{18:0}$ were done on a GC-C-IRMS system consisting on a Thermo Scientific Isotope Ratio Mass Spectrometer Delta V Advantage coupled to a GC Trace1310 through a Conflo IV interface with a temperature converter GC Isolink II. The equipment conditions were similar to the ones described by Jambrina-Enríquez et al.[13,14] Chromatography used a Trace Gold 5-MS (Thermo Scientific) capillary column (30 m length, 0.25 mm i.d. and 025 μm phase thickness), and Helium as carrier gas (1.2 mL/min). The temperature program comprised a 2 min isothermal period at 70°C, followed by an increase to 140 °C at a heating rate of 12°C/min and held for 2 min. Finally, the temperature increased from 140°C to 320 °C at a heating rate of 3°C/min and held for 15 min. The combustion reactor temperature was maintained at 1000°C. 1 μL of each sample was injected in splitless mode using a Programmed Temperature Vaporising (PTV) injector. In the evaporation stage the temperature of PTV increased from 60°C to 79°C (held 0.05 min, rate 10°C/min), followed by a transfer stage with temperature increasing to 325°C (held 3 min, rate 10°C/s) and a cleaning stage with temperature increasing to 350°C (held 3 min, rate 14°C/s). Each sample was measured in triplicate and standard deviations better than or equal to ±0.4‰ were obtained. Isotopic results are reported in the "Delta" notation as ‰ relative to Vienna Pee Dee Belemnite (VPDB). A FAME standard mixture with known $\delta^{13}C$ values ($C_{14:0}$ methyl ester to $C_{20:0}$ ethyl ester, Arndt Schimmelmann Biogeochemical Laboratories, Indiana University) was chosen to normalize the ^{13}C signal on the Vienna Pee Dee belemnite (VPDB) scale. $\delta^{13}C_{18:0}$ - $\delta^{13}C_{16:0}$ values were corrected taken into account the C introduced by methanol during methylation using the mass balance equation of Goodman and Brenna[64]

Identification and quantification

The compounds were identified based on characteristic ions and by comparing their mass spectra with those of reference compounds (mix C_8–C_{40} for F1 and 37 component FAME mix C_4–C_{24}, $C_{26:0}$, $C_{28:0}$ and $C_{30:0}$ for F5) and comparison with the Mass Spectra Database v.14. Quantification was carried out taking the four most intense fragment ions (*m/z*: 43, 57, 71 and 85 for n-alkanes; *m/z*: 67, 95, 81 and 245 for 5α-androstane; m/z: 239, 357, 359 dehydroabietic acid TMS) and the total ion chromatogram for the rest of the analytes. Quantification of F1 (*n*-alkanes) and F5 (*n*-fatty acids) compounds was based on calibration curves (r > 0.995) obtained by plotting the area/area$_{IS}$ ratio versus the concentration of each reference compound. Amount of F2, F3 and F4 compounds was estimated by comparison of peak areas with those of known quantities of 5α-androstane (F2 and F3) and 5α-androstan-3β-ol (F4). Concentrations are expressed as μg of individual compound per gram of dry sample (μg/gds).